Delineating In-Vivo T1-Weighted Intensity Profiles Within the Human Insula Cortex Using 7-Tesla MRI

AUTHOR BLOCK: *C. DALBY[1], A. DIBBLE[1], J. CARVALHEIRO[1], F. QUEIRAZZA[2], M. SEVEGNANI[3], M. HARVEY[1], M. SVANERA[1], A. FRACASSO[1]

[1]School of Psychology & Neuroscience, Univ. of Glasgow, Glasgow, United Kingdom;

[2]School of Health & Wellbeing, Univ. of Glasgow, Glasgow, United Kingdom;

[3]School of Computing Science, Univ. of Glasgow, Glasgow, United Kingdom

Corresponding author

Alessio Fracasso

Hillhead Street 62

G12 8QE

University of Glasgow, Scotland UK

Email: alessio.fracasso@glasgow.ac.uk

Statements and Declarations

Nothing to disclose.

Acknowledgements

A.F. was supported by a grant from the Biotechnology and Biology Research Council (BBSRC, grant number: BB/S006605/1) and the Bial Foundation (Bial Foundation Grants Programme; Grant id: A-29315, number: 203/2020, grant edition: G-15516).

C.D was supported by a PhD grant by the Medical Research Council (MRC) as part of the Precision Medicine Doctoral Training Programme.

A.D was supported by a PhD grant from the Scottish Graduate School of Social Science, Doctoral Training Partnership (SGSSS-DTP), on behalf of the Economic and Social Research Council (ESRC, grant number: ES/P000681/1).

Data availability: original data will be made available upon publication.

Keywords: INSULA; CORTICAL DEPTH DEPENDENT MRI; T1-WEIGHTED SIGNAL; MYELIN; HIGH-FIELD IMAGING; 7T

Abstract

The integral role of the insula cortex in sensory and cognitive function has been well documented in humans, and fine anatomical details characterising the insula have been extensively investigated ex-vivo in both human and non-human primates. However, in-vivo studies of insula anatomy in humans (in general), and within-insula parcellation (in particular) have been limited. The current study leverages 7 tesla magnetic resonance imaging to delineate T1-weighted intensity profiles within the human cortex, serving as an indirect proxy of myelination. Our analysis revealed two separate clusters of relatively high and low T1-weighted signal intensity across the insula cortex located in three distinct cortical locations within the posterior, anterior, and middle insula. The posterior and anterior cortical locations are characterised by elevated T1-weighted signal intensities, contrasting with lower intensity observed in the middle insular cortical location, compatible with ex-vivo studies. Importantly, the detection of the high T1-weighted anterior cluster is determined by the choice of brain atlas employed to define the insular ROI. We obtain reliable in-vivo within-insula parcellation at the individual and group levels, across two separate cohorts acquired in two separate sites (n1 = 21, Glasgow, UK; n2 = 101, Amsterdam, NL). These results reflect new insights into the insula anatomical structure, in-vivo, while highlighting the use of 7 tesla in neuroimaging. Specifically, the current study also paves the way to study within-insula parcellation at 7 tesla and above, and discusses further implications for individualised medicine approaches.

Graphical Abstract

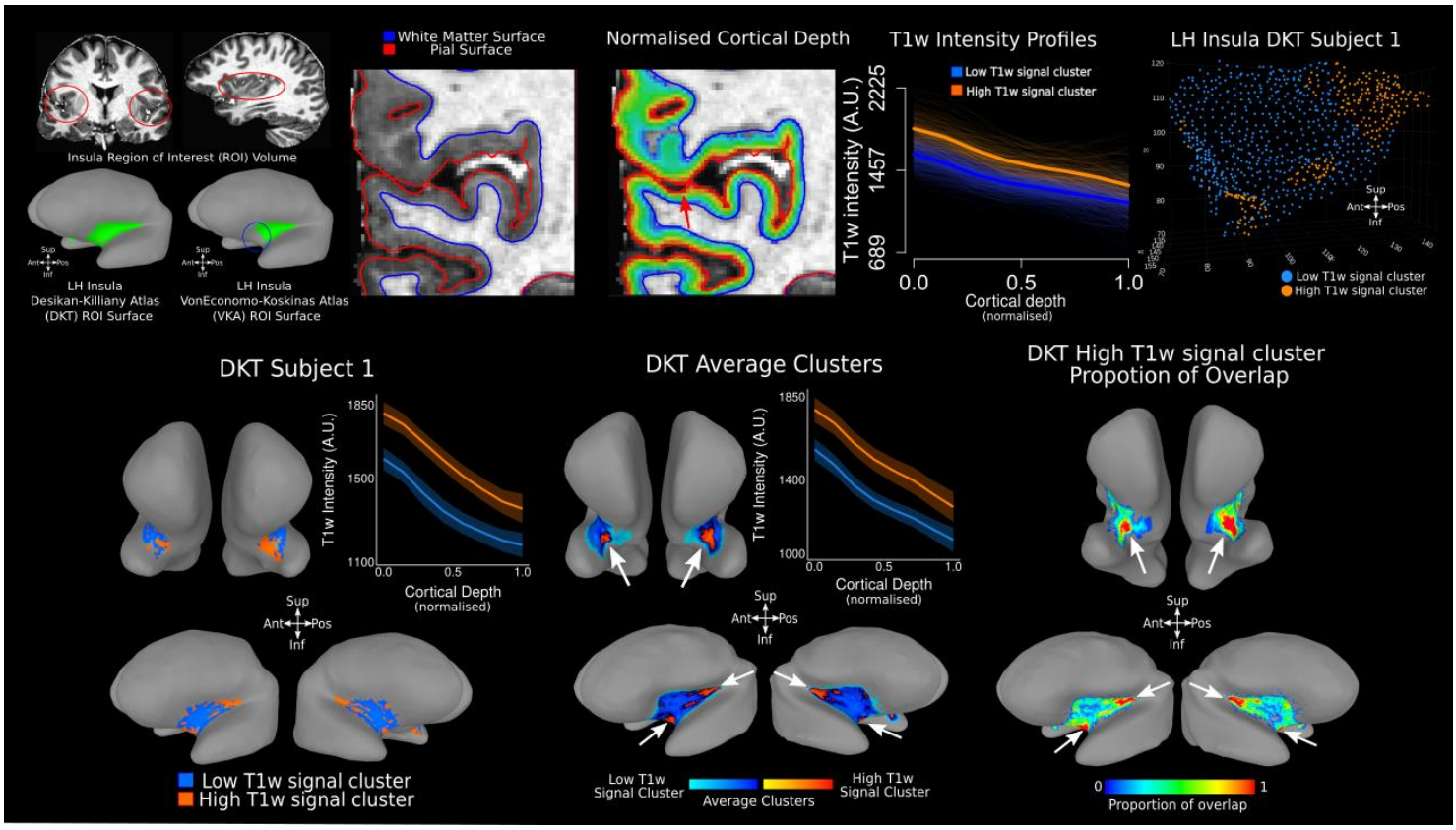

Introduction

Folded deep within the lateral sulcus of each hemisphere, the insula cortex stands as a cornerstone of human function and behaviour (Menon et al., 2020; Gasquoine, 2014). It orchestrates activity that spans the domains of sensory perception (interoception, pain, gustation), emotional regulation (empathy, social emotions), and cognitive functions (goal-directed tasks, risk, memory and language) (Craig, 2002; Craig, 2004; Critchley et al., 2004; Critchley & Garfinkel, 2017; Critchley & Harrison, 2013). Such diversity in function has even prompted speculation about the insula's candidacy for a central role in consciousness and self-awareness (de Haan et al., 2021; Medford & Critchley, 2010; Tisserand et al., 2023). Anomalies in the insula's function have been coupled with clinical disorders such as schizophrenia, frontotemporal dementia, addiction, chronic pain and inflammation (Droutman et al., 2015; Gebhardt & Nasrallah, 2023; Labrakakis, 2023). Advancing our comprehension of the insula's underlying microstructure promises insights into both the normative landscape of human behaviour and the mechanistic, diagnostic, and therapeutic dimensions of clinical populations (Benarroch, 2019).

Over the years, several attempts have been made to parcellate the insula into smaller subdivisions. Early attempts relied on Brodmann's seminal work on the distribution of neuronal bodies within human grey matter (cytoarchitectonics) (Brodmann, 1909; Geyer & Turner, 2013; Kurth, Zilles, et al., 2010), and subsequent research draws parallels with macaque cytoarchitecture, categorising the insula into granular, dysgranular, and agranular zones for posterior, intermediate, and anterior regions, respectively (Evrard, 2019; Nieuwenhuys, 2012a; Uddin et al., 2017). Similarly, immunohistochemical staining on macaque tissue by Gallay et al. (2012) revealed a ventral-to-dorsal increase in myelination. More recently, structural and functional distinctions between the insula's posterior, ventral anterior, and dorsal anterior regions have been identified - the tripartite insula subdivisions (Menon et al., 2020; Uddin et al., 2017). Utilising diffusion MRI and functional connectivity, researchers have identified white matter tracts that connect each component of the tripartite insula subdivisions to frontal, limbic, and sensorimotor regions, facilitating the differential sensory, emotional, and cognitive functions, respectively (Klugah-Brown et al., 2023; Kurth, Zilles, et al., 2010; Menon et al., 2020; Nomi et al., 2018; Uddin et al., 2017).

Furthermore, recent studies investigating the microstructure of the insula highlight the dynamic organisation of the region wherein information flows in a structured manner across its tripartite subdivisions. This process transitions from unimodal areas, which handle specific types of sensory information, to transmodal locations that integrate diverse sensory, emotional and cognitive inputs moving in anterior-ventral direction (Evrard, 2019; Royer et al., 2020). Moreover, the observed overlap in activation and the crosstalk among intra-insula regions, as discussed by Evrard (2019) and Uddin et al. (2014), suggest that these interactions underscore the insula's role as a central hub for the integration of information, culminating in complex emotional and cognitive function.

Recent advancements, exemplified by Royer et al. (2020), have expanded on this work by employing human T1/T2-weighted image intensity (T1/T2-w) as a proxy for cortical myeloarchitecture – the study of myelinated fibres distribution within grey matter (Geyer & Turner, 2013; Stüber et al., 2014; Vogt, 1903). This novel approach unveiled two major gradients in myelination: one from anterior to posterior portions of the human insula, also linked to post-mortem human cytoarchitecture (Kurth, Zilles, et al., 2010), and possibly mirroring a shift from sensory to affective functions (Uddin et al., 2014). A second myeloarchitectonic gradient was observed running in the dorsal-to-ventral direction within the human insula, potentially linked to shifts between attention and cognition (Molnar-Szakacs & Uddin, 2022; Royer et al., 2020).

In this paper, we contribute further evidence to the structural tripartite subdivision of the human insula by leveraging the higher signal-to-noise ratio and acquisition resolution that can be achieved with human high-field imaging (7T). We measure sub-millimetre T1-weighted (T1-w) magnetisation prepared rapid acquisition gradient recalled echo (MP2RAGE) images as a proxy of myelination and iron (Fukunaga et al., 2010; Stüber et al., 2014). We implemented an analysis pipeline that allowed us to gain access to cortical-depth dependent information from the human insula (Fracasso et al., 2016a, 2016b, 2018, 2021; Waehnert et al., 2014, 2016). We then derived T1-w profiles along cortical depth and used them to parcellate the human insula into locations of high- and low- T1-w intensity. We demonstrate remarkably stable parcellations at the individual subject level, for the left and right insula. We applied the same pipeline for two independent datasets, across different age-groups, acquired from two different sites and scanner vendors (n1 = 21, Glasgow, UK; n2 = 101, Amsterdam, NL).

Methods

Subjects

This study involved two cohorts. The first comprises 21 subjects (Glasgow: age range: 23-38, 10 male) recruited from Glasgow University pool of subjects. The second cohort includes 101 subjects from the AHEAD dataset, Amsterdam (age range: 18-80, 45 male, see Alkemade et al., (2020) for more details). Glasgow: all experimental procedures were approved by the local ethics committee at the School of Medical, Veterinary and Life Sciences of the University of Glasgow (reference number: 200180191 and GN19NE455). Inclusion criteria specified healthy adults from any range with no underlying neurological conditions. All subjects provided informed consent. See Alkemade et al., 2020 for experimental procedures and ethics approval of the AHEAD dataset.

MRI Acquisition

Glasgow

MRI data was acquired on a 7T Siemens Magnetom Terra system (Siemens Healthcare, Erlangen, Germany) and a 32-channel head coil (Nova Medical Inc., Wilmington, MA, USA) at the Imaging Centre of Excellence (University of Glasgow, UK). We collected T1-weighted MP2RAGE anatomical scans for each subject (0.625 mm isotropic, FOV = 160×225×240 mm^3, 256 sagittal slices, TR = 4.68 ms, TE = 0.00209s, TI = 840 ms, TI1 = TI2 = 2.37, flip angle 1 = 4, flip angle 2 = 4, bandwidth = 250Mhz, acceleration factor = 3 in primary phase encoding direction). Total acquisition time was 12 minutes.

Amsterdam

MRI data was acquired on Philips Achieva 7 MRI scanner (Philips Healthcare, Best, The Netherlands) and a 32-channel head array coil (Nova Medical Inc., Wilmington, MA, USA) at the Spinoza centre for Neuroimaging (Amsterdam, the Netherlands). T1-weighted scans for each subject were collected using a modified MP2RAGE sequence (MP2RAGEME, Caan et al., 2019), 0.7mm isotropic, FOV=205x205x164 mm3, 205 sagittal slices, TR=6.2ms, TE=0.00300s, TI=670ms, flip angle 1 = 4, flip angle 2 = 4, bandwidth = 404.9 MHz, acceleration factor SENSEPA = 2. Total acquisition time was 19.53 minutes.

Image Processing and Analysis

Data processing was conducted using Freesurfer (https://surfer.nmr.mgh.harvard.edu/), AFNI /SUMA (https://afni.nimh.nih.gov/pub/dist/doc/htmldoc/index.html), nighres, (https://nighres.readthedocs.io/en/latest/) and R (https://www.r-project.org/).
For each subject, we first skull stripped the MP2RAGE image, applying the AFNI function `3dSkullStrip` to the second inversion image (Figure 1A). The skull stripped anatomy was processed with the `recon-all` Freesurfer pipeline. Freesurfer output was converted into a SUMA compatible folder, using the command `@SUMA_Make_Spec_FS` for visualisation and processing (Figure 1A). We performed volumetric layering and profiling on the original isotropic MP2RAGE (Figure 1B).

Cortical Depth Analysis

We used nighres (Huntenburg, Steele and Bazin, 2018) to process the automatic segmentation of the anatomical (T1-w, MP2RAGE) images. We generated white matter and grey matter level-sets using the nighres function `surface.probability_to_levelset()`. A volume-preserving distance map was computed between the white matter/grey matter boundary and the grey matter/cerebro-spinal fluid boundary in 8 separate level-set volumes (Figure 1C,D) using the nighres function `laminar.volumetric_layering()`. This equi-volume model provides a coordinate system of cortical depth which is independent from local cortical folding (Fracasso et al., 2018, 2021; Waehnert et al., 2014, 2016). Cortical thickness and cortical curvature were estimated using Freesurfer. For each voxel within grey matter, a cortical depth profile of T1-w intensity was generated following the equi-volume metric and stored for subsequent analysis using the nighres function `nighres.laminar.profile_sampling()`, see Figure 1E.

Region Of Interest (ROI) Definition

We derived the insula ROI from two separate atlases to test the robustness of the proposed pipeline against different ROI definitions: i) the Desikan-Killiany atlas (Desikan et al., 2006), as it is widely used in the neuroimaging literature and ii) the Von Economo-Koskinas Atlas (Scholtens et al., 2018), as it has been used in a previous investigation focusing on characterising myelin gradients within the human insula (Royer et al., 2020).

Desikan-Killiany Atlas (DKT)

The atlas developed by Desikan et al., (2006) is a surface-based parcellation scheme for the human cerebral cortex. It was created using a dataset of 40 MRI scans to define cortical regions of interest (ROIs). The authors employed a semi-automated approach that combined manual labelling of specific cortical landmarks (sulcal representation) with automated parcellation algorithms (Fischl et al., 2004). The resulting atlas divides the

cerebral cortex into 34 distinct ROIs per hemisphere, providing a standardised framework for structural and functional analyses. Later, the original Desikan-Killiany atlas was refined and a more detailed and consistent labelling protocol was developed, leveraging 101 brain images from the Mindboggle-101 dataset (Klein & Tourville, 2012). Regarding the insula cortex, the atlas defines a single insula ROI for each hemisphere without further subdivision into subregions.

Von Economo-Koskinas Atlas (VKA)

The Von Economo-Koskinas atlas, originally published in the early 20th century, is a comprehensive brain atlas that parcellates the human cerebral cortex based on cytoarchitectonic differences observed in the cellular structure and organisation of the cortical layers (Economo & Koskinas, 1925). Created by Constantin von Economo and George Koskinas, this atlas was developed through meticulous microscopic examination of stained brain sections. The atlas divides the cerebral cortex into numerous cytoarchitectonic areas, each characterised by distinct patterns of cellular organisation and density. Regarding the insula cortex, the Von Economo-Koskinas atlas identified several cytoarchitectonic subdivisions within this region. The most notable are the agranular, granular and dysgranular insula. This granularity makes the atlas a valuable resource for understanding the structural organisation of the insula, which is critical for correlating anatomical features with function and clinical observations. Scholtens et al., (2018) modernised this historic atlas by manually segmenting the atlas on individual T1 scans and using FreeSurfer software to construct a digitised group-specific cortical parcellation atlas file. Royer et al.'s, (2020) findings were based on the digitised version of this atlas, and we also employed the same version of the VKA atlas to facilitate comparisons (Figure 1A).

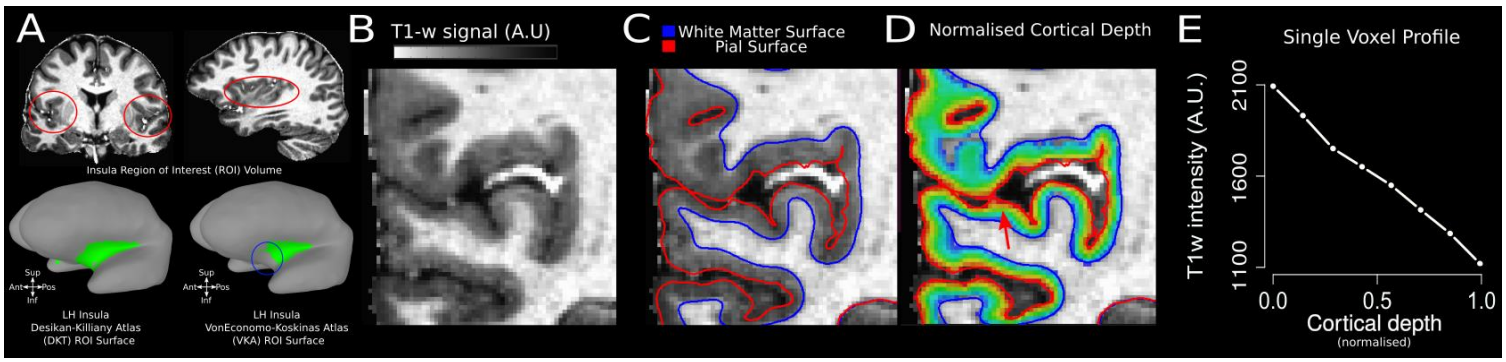

Figure 1, Pre-Processing.

A. *Insula ROI obtained from the DKT (no of voxels: 9587 mm^3) and VKA (no of voxels: 5431 mm^3) atlas. These atlases differ. Compared to the VKA, the DKT extends more towards the anterior part of the brain and dorsally with respect to the orbito-frontal cortex (see blue circle), and more towards the posterior part of the brain, towards the supramarginal gyrus.* ***B.*** *Coronal slice details of the MP2RAGE, single subject, left insula (0.7mm isotropic).* ***C.*** *Grey matter / white matter boundary (blue line) and grey matter / cerebro-spinal fluid boundary (red line).* ***D.*** *Volumetric distance map along cortical depth.* ***E.*** *Individual T1-w profile passing through the voxel highlighted by the red arrow in panel D. T1-w signal is at its peak close to the white matter (0 on the x axis), then sharply decreases approaching the cerebro-spinal fluid (1 on the x axis).*

Differences between DKT and VKA Insula ROI

It became quickly apparent that the insula ROI defined from the DKT atlas differed from the insula ROI obtained from the VKA atlas. Namely, the former extends more towards the anterior part of the brain (Figure 1A), dorsally with respect to the orbito-frontal cortex. Moreover, DKT insula ROI (9587 mm^3) extends more towards the posterior part of the brain and the supramarginal gyrus compared with the VKA atlas insula ROI (5431 mm^3). This difference between the two atlases can be ascribed to the different criteria used to define ROIs in each atlas. The DKT atlas adopted a sulcal approach, based on manually tracing from one sulcus to another, incorporating the gyrus in between (Desikan et al., 2006; Klein & Tourville, 2012). On the other hand, the VKA atlas is based on the original work on Von Economo and Koskinas (Economo & Koskinas, 1925; Scholtens et al., 2018), which relies on cytoarchitectonics: the distribution of neuronal bodies within human grey matter. Given the different criteria adopted in the definition of the two atlases, it is not surprising to notice differences in ROI boundaries. In the current manuscript we are not interested in providing an evaluation of which atlas best captures the insula, and we remain agnostic on the matter. Here, we are interested in providing a characterisation of intra-insular parcellation using T1-w signal along cortical depth. For this reason, we opted to highlight the results using both atlases (DKT and VKA), assessing potential differences between the two.

Removing Cortical Curvature and Cortical Thickness Contributions

For each subject and insula ROI (VKA and DKT), we loaded T1-w data in R using the function `read.AFNI()` from the file AFNIio.R from AFNI. To increase signal-to-noise ratio and minimise the potential contribution of small grey matter segmentation errors, we divided each insula ROI in 1000 separate cortical location, each containing approximately 20 neighbouring voxels (range = 15-30). We averaged the T1-w profiles from each cortical location, thus obtaining 1000 averaged T1-w profiles for each subject and insula ROI. From now on, we will refer to the averaged T1-w profiles as T1-w profiles. Moreover, for each cortical location we obtained an estimate of cortical curvature and cortical thickness obtained from Freesurfer.

The human cortex is characterised by a complex pattern of concavity and convexity, and myelin content varies significantly with local cortical convexity (Annese et al. 2004). T1-w signal is known to vary systematically with cortical curvature as well as cortical thickness, convex regions tend to be thicker and more myelinated and vice-versa (Sereno et al., 2013). We removed the contributions of local cortical curvature and thickness for each level-set along cortical depth (8 level-sets overall from white matter to grey matter surface). We fit a linear model for each level-set where we factored the contribution of local cortical curvature and local cortical thickness plus the interaction between the two. For each level-set along cortical depth, we used the residuals of the linear model just described, after adding the estimated intercept T1-w signal.

Cluster Analysis

We ran a cluster analysis on the T1-w profiles (Figure 2). We adopted the k-means clustering implementation in R, using Euclidean distance as distance metric in T1-w profile space in the *k-means* function. Please note that clustering was performed on T1-w profiles only and the

algorithm did not have access to the 3D coordinates -XYZ- of individual voxels. To determine the optimal number of clusters, we inspected the silhouette score of the clustering solution, using the function `fviz_nbclust`, from the library *factoextra* in R. For any given entry in the set, the silhouette score measures how similar an entry is to its own cluster compared to other clusters. The silhouette score ranges from -1 to 1. Values above 0 indicates that the entry is well matched to its own cluster and poorly matched to neighbouring clusters. The opposite is true for values below 0. The silhouette score for the entire dataset is the average of the silhouette scores of all individual entries. The plot of silhouette score across different number of clusters provides a way to visually assess the optimal number of clusters. We have generated a separate silhouette plot for each subject and insula (left and right hemisphere). Moreover, we derived the average silhouette plot from individual silhouette plots for a number of clusters ranging between 1 and 10.

Surfaces

We used the standard-mesh approach in SUMA (AFNI) to visualise data at the individual and average population level. A standard-mesh version of a surface is virtually an identical 3D mesh of the individual; however, this approach has the advantage that each node of the new mesh represents the same cortical location across subjects. The original subject's mesh is recreated using the template mesh, instead of mapping a subject's data value onto the template mesh (Saad & Reynolds, 2012). For each subject and insula ROI (VKA and DKT), we projected the k-means output and sorted the output by their average T1-w intensity. We plot the separate clusters on individual subjects' surfaces using a categorical variable. Moreover, we plot the proportion of overlap or each sorted cluster across the population. For each node in the insula ROI, we computed the proportion of subjects for which that specific node was labelled with the same cluster (ranked). This results in an overlap map, showing the consistency of insula parcellation across the population.

DKT Atlas, The Influence of The Middle Cerebral Artery on T1-w Signal Intensity

The middle cerebral artery (MCA) is a major artery supplying blood to the lateral portion of the cerebral cortex, including the primary motor and sensory areas. Originating from the internal carotid artery, it runs laterally through the Sylvian fissure, closely adjacent to the insula cortex (Medrano-Martorell et al., 2021). The M2 segment of the middle cerebral artery refers to the portions of this artery that course laterally beyond the insula, branching extensively within the Sylvian fissure. This segment represents the continuation of the MCA after it traverses the surface of the insula, where it bifurcates or trifurcates into smaller arteries that supply cortical regions adjacent to and beyond the insula (Tanriover et al., 2004). Thus, while the M2 segment directly follows the insular traversal of the MCA, it is primarily involved with vascularising areas external to the insula itself (Türe et al., 2000).

Crucially, large arteries as MCA and their associated branches appear as bright tubular structures in T1-w images. Such a high T1-w signal intensity in proximity with the superficial grey matter border could bias T1-w profiles. To assess the influence of MCA in the T1-w signal profiles we display the grey matter location of MCA with respect to our clustering results, and statistically assess differences in our clustering results that might be ascribed to MCA proximity.

Analysis

DKT Atlas, MCA influence

For the DKT atlas, we assessed the influence of MCA proximity to our clustering solution using a linear model, fitting the relationship between T1-w signal and normalised cortical depth, using cluster location as a categorical variable. We test the differences between separate clusters in terms of intercept (T1-w value at the white matter interface) and slope (rate of change of T1-w signal rate per unit change of cortical depth).

Stability of insula cluster maps

We assessed the stability of insula cluster maps using a leave-one-out procedure. For each iteration, we computed the average cluster map from n-1 individuals and tested the similarity between the n-1 average and the nth individual insula map using a logistic regression model and the logit function as link. For each individual and insula, we obtained the corresponding t statistic and p-value, representing how well the n-1 average cluster map captured the variability in the individual insula map. Building on the estimates of the logistic regression model, we computed the areas-under-the-curve (AUC) within a receiver-operating-characteristic curve (ROC) framework for each subject and insula. We report the AUC value and associated D-prime for each subject and insula in our dataset. D-prime is a measure derived from signal detection theory (Hautus et al., 2021) to quantify the ability to discriminate between two distributions, in this case between the distribution of separate clusters. D-prime represents the separation between the means of two distributions, standardised by their standard deviations. A value of 1 indicates a level of discriminability following approximately a hit-rate of 75% and a proportion of false-alarms of 30%.

Clusters or gradient

When discussing clusters in any modality, it is necessary to acknowledge that what might appear to be separate clusters, could instead be a continuous gradient. After thresholding by any clustering algorithm, a continuous gradient could be interpreted as separate clusters. On the other hand, 'true' separate clusters should be identified by a sudden change (a transient) in properties when transitioning from one cluster to another. To disentangle between the 'cluster' and the 'gradient' alternatives, we performed the following analysis. Inspecting clustering output at the T1-w profile level, it became apparent that different clusters were defined by different offsets. For this reason, for each subject and insula ROI, we projected on the MNI surface the T1-w profile intercept of each T1-w profile.

We reasoned that a gradient between the two separate clusters would manifest as a linear change in T1-w profile intercept along the underlying cortical distance between the clusters. On the other hand, a transient change in T1-w profile intercept along the cortical distance between clusters should be better approximated by a stepwise function. Please note that we use the term 'cortical distance' referring to the geodesic distance over the cortical surface, i.e. the shortest path between vertices over the cortical surface. We manually drew ROIs, crossing the border between neighbouring clusters on the MNI surface space and computed the corresponding geodesic distances within the ROI.

We computed the vertex-to-vertex geodesic distance from each node within the ROI – the adjacency matrix. We computed the spectral decomposition of the adjacency matrix and selected the first eigenvector of the decomposition. This vector represents a map of cortical distance over the ROI along its longest axis, where each point in the map is the geodesic distance of a node along the selected axis with respect to 0 – the middle of the ROI along its longest axis (Fracasso et al., 2021; Grady & Polimeni, 2010; Lombaert et al., 2011). This cortical distance (or geodesic distance) provides a common reference frame against which we can test the linear (gradient) versus stepwise (cluster) hypothesis.

We plotted the T1-w profile intercept along the cortical distance, and statistically assessed whether the data could be best fit by a linear or stepwise relationship. We tested a linear relationship fitting two parameters: an intercept and a slope (Eq. 1).

Eq. 1 $T1w_{intercept} = intercept + cd \cdot slope$

Where *cd* is cortical distance.

We used a cumulative Gaussian function with three parameters (multiplicative factor – mult -, shift and sigma, eq. 2) to test the stepwise alternative.

Eq. 2 $T1w_{intercept} = mult \cdot \left(\frac{1}{2}\left[1 + erf \cdot \frac{cd}{\sigma\sqrt{2}}\right]\right) + shift$

We compared the goodness of fit between the two models (linear and cumulative Gaussian) using the AIC criterion, penalising for the difference in the number of parameters between the two models (two against three). Statistical analyses and model fits were performed using R (https://www.r-project.org/).

AHEAD dataset

We performed the same processing and analyses for the AHEAD dataset (Alkemade et al., 2020). See section Results for further details.

Results

T1-w Cortical-Depth Dependent Profiles of the Human Insula

First, we present our results on the Glasgow dataset (21 subjects). These are followed by the results from the AHEAD dataset (Alkemade et al., 2020). For each dataset, here we present the results obtained from the DKT atlas, followed by the results of the VKA atlas. Following preprocessing, T1-w signal profile sampling (Figure 1A-E) and clustering (Figure 2), our analysis reveals two distinct profiles of low and high T1-w intensity, respectively (Figure 2). Qualitatively, using the DKT insula ROI, high T1-w intensity profiles tended to be localised in the anterior-inferior and posterior-superior insular locations (Figure 3).

Cluster Analysis on T1-w Profiles

K-means clustering and a silhouette plot (Figure 2) evidence the optimal number of clusters for dividing T1-w intensity profiles in the insula across both left and right hemispheres. For average (21 participants) and three individual subjects' examples, the mean silhouette score peaks at two clusters and monotonically declines thereafter. This indicates that two clusters is the optimal solution at the individual insula level as well as across subjects. Should the

optimal number of clusters be different (six clusters, for example), we would expect to see a peak in silhouette score at six, with a subsequent decrease, as the number of clusters increases.

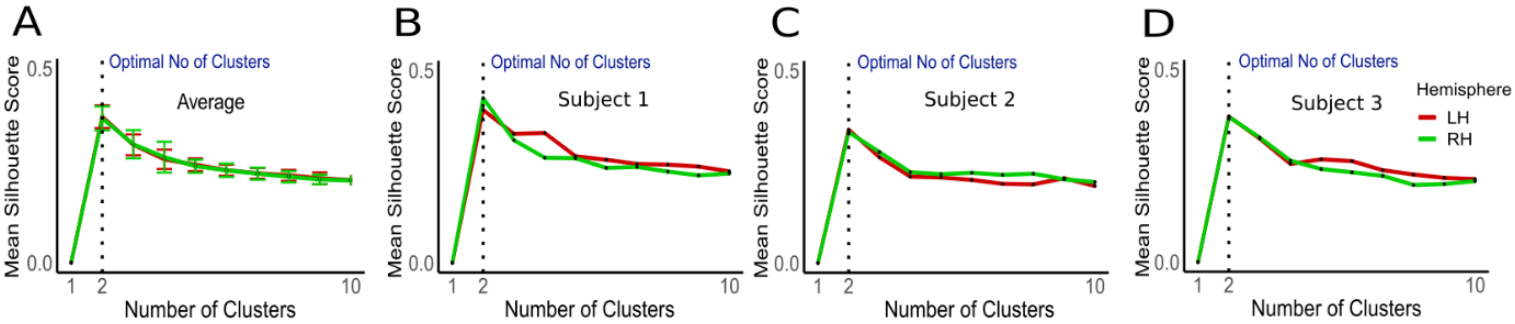

Figure 2, Silhouette Plots of K-Means Clustering Solution.
A. *Average silhouette plot for the left (red line) and right (green line) hemisphere DKT insula ROI across all 21 subjects, Glasgow dataset. Number of tested clusters ranged from 1-10. Dotted line indicates the optimal number of clusters (2). Error bars around each line indicate variability (+/- 1 standard deviation).* ***B-D.*** *Silhouette plots for three subjects to exemplify the optimal cluster number (2) remains consistent at the individual subject level.*

In the following figure (Figure 3), we qualitatively report K-means clustering results, on two subjects.

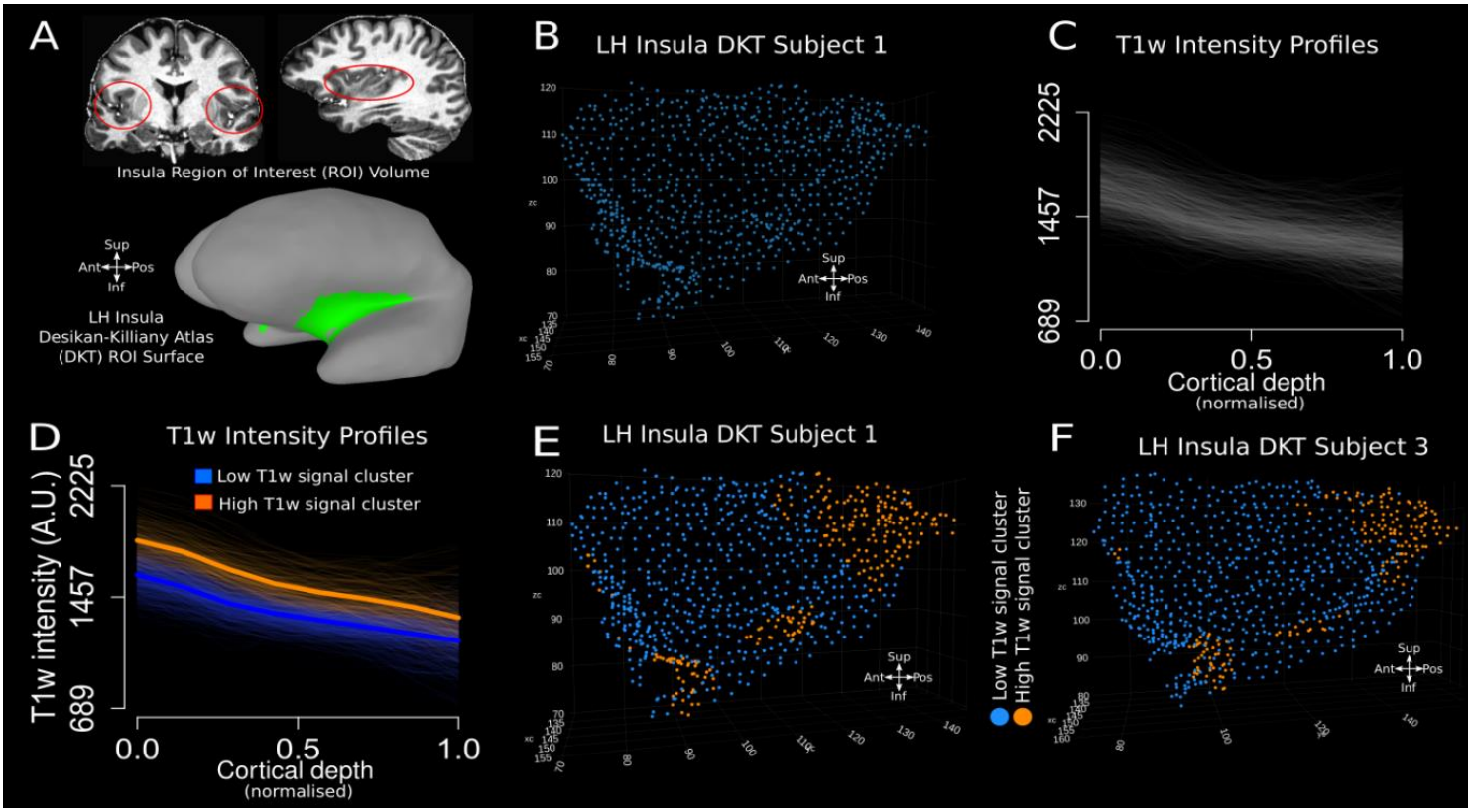

Figure 3, Individual Insula Clustering.
A. *Insula ROI obtained from the DKT (no of voxels: 9587 mm^3) atlas as viewed on the T1-w MRI volume (panel 1 and 2; red circles) and SUMA surface (green shading).* ***B.*** *Representation of the left insula in individual subject native space. Blue points in 3D space represent the 1000 T1-w profiles, each resulting from the average of ~20 voxels, ROI=DKT.* ***C.*** *individual T1-w profiles from the same insula from panel B.* ***D.*** *K-means clustering results, separating high T1-w profiles from low T1-w profiles. Please note that a clustering analysis indicated 2 as the optimal solution. See the Results section: 'Cluster Analysis on T1-w Profiles'.* ***E,F.*** *High T1-w profiles and low T1-w profiles colour coded on two individual subjects in native space (left insula). Qualitatively, in these two insula ROIs (from DKT atlas), the high T1-w intensity profiles tend to be localised in the anterior-inferior and posterior-superior insular locations.*

T1-w Intensity Profiles and Clusters on the DKT Insula ROI

Our analysis revealed distinct high- and low-T1-w intensity profiles across DTK insula ROI, at an individual (Figure 3 and Figure 4A, B) and group level (Figure 4C). T1-w signal monotonically decreases along cortical depth in both the high- and low-T1-w signal cluster (estimate = -487.65, t=21.10, p<0.001). Average T1-w profiles along cortical depth for individual subjects show how clusters differ predominantly on their offset (intercept with respect to the white matter border), rather than their slope (rate of change along cortical depth) (Figure 4A-C). Statistical analysis confirms this difference in intercept (estimate = 144.20, t=21.10, p<0.001) without a change in slope (estimate =-4.94 t=-0.43, p=0.67) between the high and low T1-w intensity profiles. Crucially, the profiles in the high T1-w signal cluster can be found in two separate cortical location along the DKA insula ROI: in the posterior-superior portion and the anterior-inferior portion of the DKA insula ROI (Figure 4C,E). On the other hand, the profiles in the low T1-w signal cluster can be found in the middle of the DKA insula ROI, between the

high T1-w signal profiles in the posterior-superior portion and those in the anterior-inferior portion of the DKA insula ROI (Figure 4D).

The location of high and low T1-w clusters is consistent between individuals. More than 70% of individuals show high T1-w intensity clusters localised towards the anterior-inferior and posterior-superior DKT insula ROI (Figure 4C,E white arrows) and the low T1-w intensity cluster is localised in the middle region of the DKT insula ROI (Figure 4D). Across the population, the high T1-w clusters location occupy 28% of the DKT surface insula ROI (here we defined a high T1-w cluster location across the population as those nodes on the cortical surface where more than 70% of individuals show a high T1-w intensity cluster).

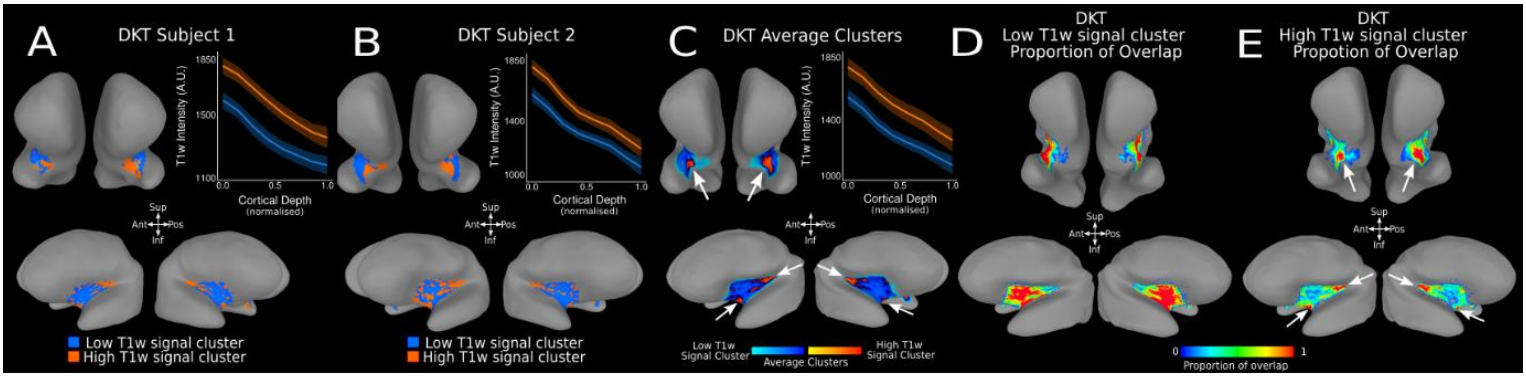

Figure 4, T1-w Intensity Profiles and Clusters in DTK insula ROI.
A-B. *Average high (orange) and low (blue) T1-w intensity profiles for the insula DKT ROI at the individual subject level. T1-w intensity is plotted along cortical depth and clusters are visualised on the MNI SUMA surface of the individual's cortex (high T1-w intensity cluster – orange – and low T1-w intensity cluster – blue –).* ***C.*** *Average high (orange) and low (blue) T1-w intensity profiles for the insula DKT ROI across 21 subjects. T1-w intensity is plotted across cortical depth and average clusters across 21 subjects are visualised on the SUMA MNI surface. White arrows identify two areas of high T1-w signal clusters, located in the posterior-superior and anterior-inferior region of the DKT insula ROI.* ***D.*** *Proportion of overlap for low-T1-w signal cluster within the insula DKT ROI across 21 subjects, visualised on the average MNI SUMA surface.* ***E.*** *Proportion of overlap for high T1-w signal cluster for the insula DKT ROI across 21 subjects visualised on the MNI SUMA surface. White arrows identify two areas of high overlap for high-T1-w signal cluster, located in the posterior-superior and anterior-inferior region of the DKT insula ROI.*

Atlas Selection Governs Detection of Anterior T1-w Cluster

Following the results using the DKT atlas, we then aimed to replicate our findings in the VKA atlas employed by (Royer et al., 2020). Distinct high- and low-T1-w intensity profiles are also evident across the VKA atlas insula ROI at an individual level (Figure 5A,B) and group level (Figure 5C). As with the DKT atlas, T1-w signal monotonically decreases along cortical depth in both the high- and low-T1-w signal cluster (estimate = -469.40, t=-529.13, P<0.001). Equally, a high-T1-w intensity cluster is localised to the posterior-superior section of the VKA insula ROI (Figure 5C,E white arrows), while the low-T1-w intensity cluster is localised in the middle-anterior region of the VKA insula ROI. Statistical analysis confirms this difference in intercept (estimate = 209.66, t=268.50, p<0.001) and in slope (estimate =-61.60 t=-47.63 p<0.001) between the high and low T1-w intensity profiles. However, we could not observe a high-T1-w intensity cluster in the anterior VKA insula ROI, due to the differences in extent towards the anterior section of the brain between the DKT and VKA insula ROI (see section "*Differences between DKT and VKA Insula ROI*"). As with the DKT surface insula, here we also define a high

T1-w cluster location across the population as those nodes on the VKA cortical surface where more than 70% of individuals show a high T1-w intensity cluster. Likely due to the previously discussed atlas differences, the high T1-w clusters location only occupy 11% of the VKA surface insula ROI, across the population.

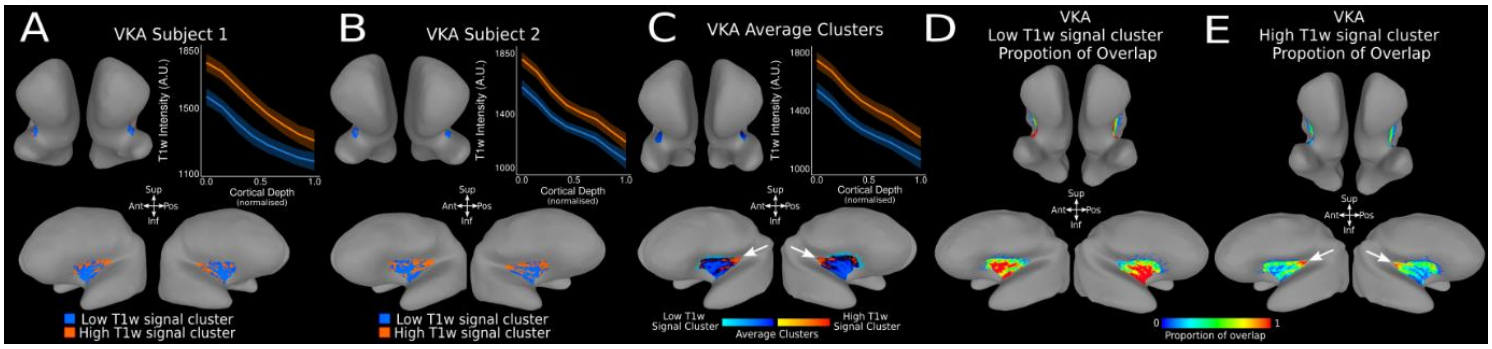

Figure 5, T1-w Intensity Profiles and Clusters in VKA Insula ROI.
A-B. *Average high (orange) and low (blue) T1-w intensity profiles for the insula VKA ROI at the individual subject level. T1-w intensity is plotted along cortical depth and clusters are visualised on the MNI SUMA surface of the individual's cortex (high T1-w intensity cluster – orange – and low T1-w intensity cluster – blue –).* ***C.*** *Average high (orange) and low (blue) T1-w intensity profiles for the insula VKA ROI across 21 subjects. T1-w intensity is plotted across cortical depth and average clusters across 21 subjects are visualised on the SUMA MNI surface. The white arrow identifies the single area of high T1-w signal clusters, located in the posterior-superior region of the VKA insula ROI.* ***D.*** *Proportion of overlap for low-T1-w signal cluster within the insula VKA ROI across 21 subjects, visualised on the average MNI SUMA surface.* ***E.*** *Proportion of overlap for high T1-w signal cluster for the insula VKA ROI across 21 subjects visualised on the MNI SUMA surface. The white arrow identifies the single area of high overlap for high-T1-w signal cluster, located in the posterior-superior region of the VKA insula ROI. High-T1-w intensity cluster in the anterior VKA insula ROI was not observed due to the differences in extent towards the anterior section of the brain between the DKT and VKA insula ROI.*

DKA Insula ROI, and Proximity to The Middle Cerebral Artery (MCA)

The profiles in the high T1-w signal cluster can be found in two separate cortical locations along the DKA insula ROI: in the posterior-superior portion and the anterior-inferior portion of the DKA insula ROI (Figure 4C,E). Importantly, the anterior-inferior section of the DKA insula ROI is situated near the MCA artery. Large arteries, such as MCA and their associated branches, can appear as bright tubular structures in T1-w images (Figure 6). Such a high T1-w signal intensity in proximity with the superficial grey matter border could bias T1-w profiles. Here, we report the grey matter location of the high- and low- T1-w signal cluster in individual subjects, as well as the average T1-w profile for the posterior-superior, middle and anterior-inferior T1-w signal insular clusters (Figure 6), and their position with respect to MCA at the individual subject level. We report the results for three individual subjects (Figure 6A-C) as well as across the population (21 subjects).

We quantitatively compared the high-T1-w signal cluster in the posterior-superior and anterior-inferior DKA insula ROI. Statistical analysis shows a difference in intercept (estimate = 87.80, t=12.64, p<0.001) and slope (estimate =-195.16 t=-16.79, p<0.001), indicating a shallower slope for the anterior-inferior high-T1-w signal cluster compared to the posterior-superior (Figure 6D). This is to be expected as partial volume influence from the MCA can contribute to increasing T1-w signal close to the pial surface for the anterior-inferior T1-w signal cluster. However, although the average T1-w profile in the anterior portion of the DKT insula ROI is statistically different from its posterior counterpart, visual inspection of the profiles (Figure 6) indicates that the presence of MCA does not disrupt the overall shape of T1-w signal profiles along cortical depth in the anterior high-T1-w signal cluster, and the high-T1-w cluster in the anterior insula is not driven by the MCA proximity.

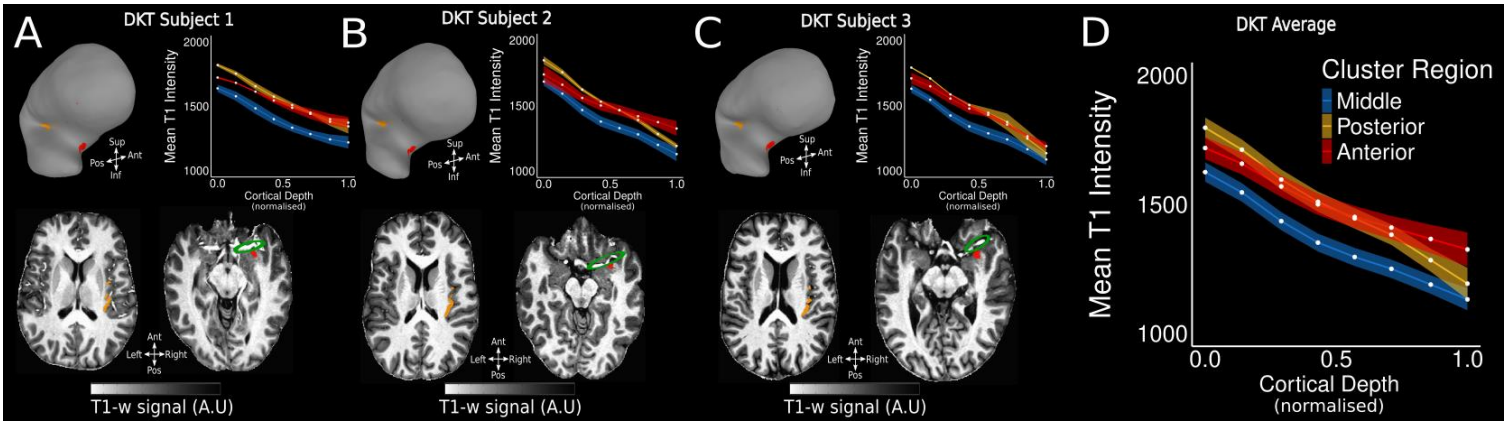

Figure 6, Proximity of the Anterior-Inferior High T1-w Cluster to Middle Cerebral Artery.
A-C. *T1-w signal clusters, located in the posterior-superior (yellow), anterior-inferior (red) and middle (blue) region of the DKT insula ROI across 3 subjects. High T1-w signal clusters are visualised on the right hemisphere SUMA MNI surface (panel 1) and T1-w intensity profiles are plotted along cortical depth (panel 2). High T1-w signal clusters are visualised on each subject's T1-w volume (panel 3-4). Green circle indicates the location of the middle cerebral artery segment.* ***D.*** *Average T1-w intensity profiles for the posterior-superior (yellow), anterior-inferior (red) and middle (blue) region of the DKT insula ROI for 21 subject plotted across cortical depth.*

T1-w Intensity Profiles are Arranged in Clusters, Not Gradients

It is important to note that any continuous gradient results in separate clusters after being thresholded by any clustering algorithm. 'True' separate clusters should be identified by a sudden change (transient) in properties when transitioning from one cluster to another. We manually drew ROIs, crossing the border between neighbouring clusters on the MNI surface space and computed the corresponding geodesic distances within the ROI (Figure 7 A,B). Different clusters are defined by different offsets (different T1-w profile intercept for the high- and low-T1-w signal clusters). For this reason, for each subject and cortical location within the insula ROI, we projected on the MNI surface the T1-w profile intercept (Figure 7C). A continuous gradient between the high-T1-w signal cluster and the low-T1-w signal cluster would manifest as a linear change in T1-w profile intercept along the cortical distance between the two clusters. On the other hand, a transient change in T1-w profile intercept along the cortical distance between clusters should be better approximated by a stepwise function (Figure 7D, blue and red curves for the linear and stepwise cumulative Gaussian fit, respectively).

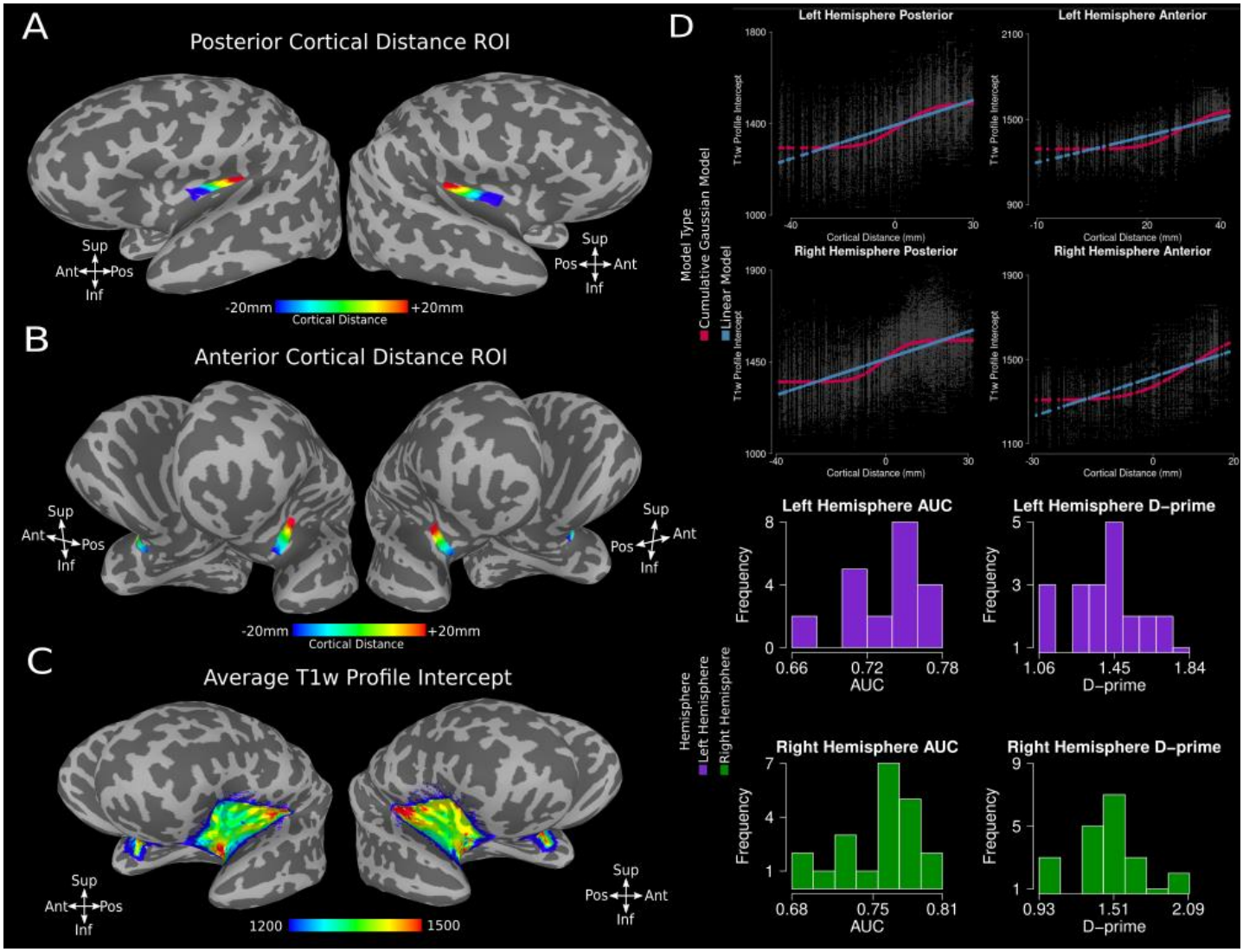

Figure 7: Gradient vs Clustering in DKT Insula ROI.
A. *Cortical distance maps for posterior insula (left and right hemisphere).* ***B.*** *Cortical distance map for anterior insula (left and right hemisphere).* ***C.*** *T1-w profiles intercept map over MNI SUMA surface for the left and right hemisphere.* ***D.*** *T1-w signal intensity intercept along cortical distance for each of the four ROI depicted in panels A,B. Original data is reported in grey, the result of the linear fit is reported in blue, the result of the cumulative Gaussian fit is reported in red (see legend). Histograms show the computed AUC and corresponding D-prime from the logistic regression analysis (see section Stability of insula cluster maps in Analysis). AUC values are above 0.5 in each individual participant, indicating the stability of the clustering results at the individual participant level. The corresponding D-prime values further support this observation, with the worst D-prime values ~1 and the most representative value being ~1.5, approximately corresponding to a hit-rate of 85% and a proportion of false-alarms of 25% in the leave-one-out scenario. See text for further details.*

To disentangle between different alternatives, we fit a linear and a cumulative Gaussian model on T1-w signal intercept over cortical distance and assessed which model best captured variability in the data. Results indicate that the cumulative Gaussian model outperforms the linear model on each of the 4 ROI across high- and low-T1-w signal clusters in the posterior and anterior insula, for each hemisphere (see Table 1).

Region	Model	AIC	BIC
LHP	Cumulative Gaussian***	236705.62	236745.05
	Linear	237773.96	237797.61
LHA	Cumulative Gaussian***	107748.69	107784.28
	Linear	109379.79	109401.15
RHP	Cumulative Gaussian***	302910.52	302951.11
	Linear	304587.00	304611.35
RHA	Cumulative Gaussian***	89478.06	89512.66
	Linear	90328.40	90349.16

*** P < 0.0001

Table 1. Summary Statistics of Linear and A Cumulative Gaussian Model on T1-w Signal Intercept Over Cortical Distance.

Region refers to the regional location within the cortex (LH-: Left Hemisphere, RH-: Right Hemisphere, -A: Anterior, -P: Posterior). Model refers to the statistical model used to capture the variability for T1-w signal intercept over cortical distance. Akaike information criterion (AIC) and Bayes information criterion (BIC) values remain consistently lower for the Cumulative Gaussian model compared to the Linear Model across brain regions, indicating a better fit. Further statistical comparison using ANOVA supported these findings with significant results (see p-values) indicating the Cumulative Gaussian model more effectively captures the variability than the Linear model.

These results indicate that the clusters we report cannot be explained by a simple gradient along the insula, but rather by a transient change in properties along cortical distance (Figure 7D). A D-prime value of 1 indicates a level of discriminability following approximately a hit-rate of 75% and a proportion of false-alarms of 30%. This indicates that in the worst case, our leave-one-out model (the average of all individuals minus one) could correctly predict whether a high-T1w profile of the left-out individual was categorised as being high-T1w intensity 75% of the time, whereas a low-T1w profile was wrongly categorised as high-on 30% of the times. We want to stress how our worst observed D-prime hovered around 1, with the most frequent value at the individual participant, individual insula level being ~1.5, corresponding to a hit-rate of 85% and a proportion of false-alarms of 25%, indicating that these are separable clusters.

AHEAD Dataset

Utilising the same analysis pipeline, we replicated the reported initial findings from 21 participants (Glasgow) in a different cohort of 101 subjects using the AHEAD dataset. Importantly, the AHEAD dataset is a multi-contrast anatomical dataset where the authors acquired data using an MP2RAGE sequence with similar parameters as the MP2RAGE sequence we used to acquire data in Glasgow (see methods for more details about the dataset).

Determining Number of Clusters for AHEAD Dataset

We applied the same k-means clustering used for the Glasgow cohort and a silhouette plot (Figure 8) to evidence the optimal number of clusters to divide T1-w intensity profiles in the insula across both left and right hemispheres. For the average (101 participants) and for three individual subjects' examples in the AHEAD dataset, the mean silhouette score peaks at two clusters and monotonically declines thereafter. This indicates that two clusters are the optimal solution at the individual insula level as well as across subjects in using the AHEAD dataset.

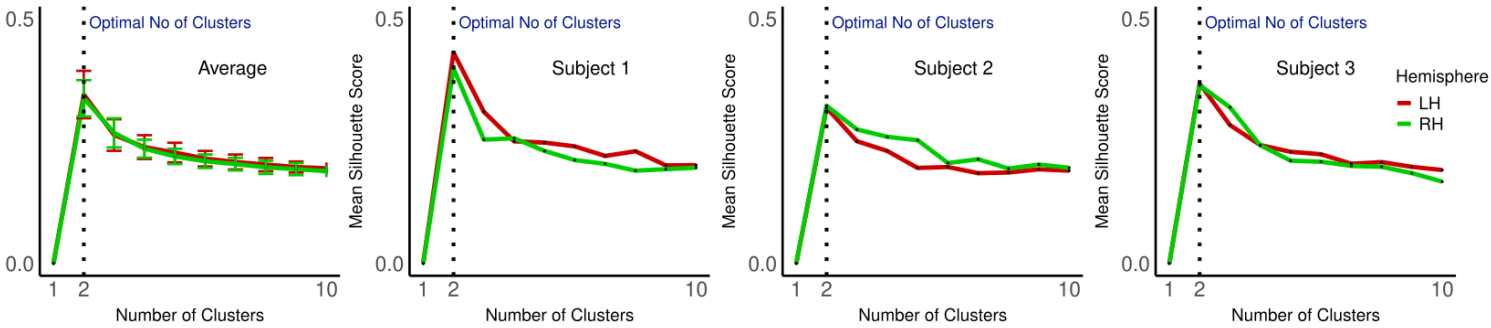

Figure 8, Silhouette Plots of K-Means Clustering Solution for AHEAD Dataset.
A. *An Average silhouette plot for the left (red line) and right (green line) hemisphere insula ROI across all 101 subjects, AHEAD dataset. Number of tested clusters ranged from 1-10. Dotted line indicates the optimal number of clusters (2). Error bars indicate variability (+/- 1 standard deviation).* ***B-D.*** *Silhouette plots for three subjects to exemplify the optimal cluster number (2) remains consistent at the individual subject level.*

Individual-Level T1-w Intensity Profiles and Clusters Within the DKT and VKA Insula ROI of the AHEAD Dataset

In line with our previous findings, our analysis revealed distinct high- and low-T1-w intensity profiles across DTK insula ROI at the individual-level (Figure 9A). T1-w signal monotonically decreases along cortical depth in both the high- and low-T1-w signal cluster. As with our previous analysis, we evidence two differently distributed but distinct high- and low-T1-w intensity profiles when employing the VKA insula ROI for the same individual (Figure 9B). We replicated these results in a second subject to exemplify the robustness of the findings (Figure 9C, D).

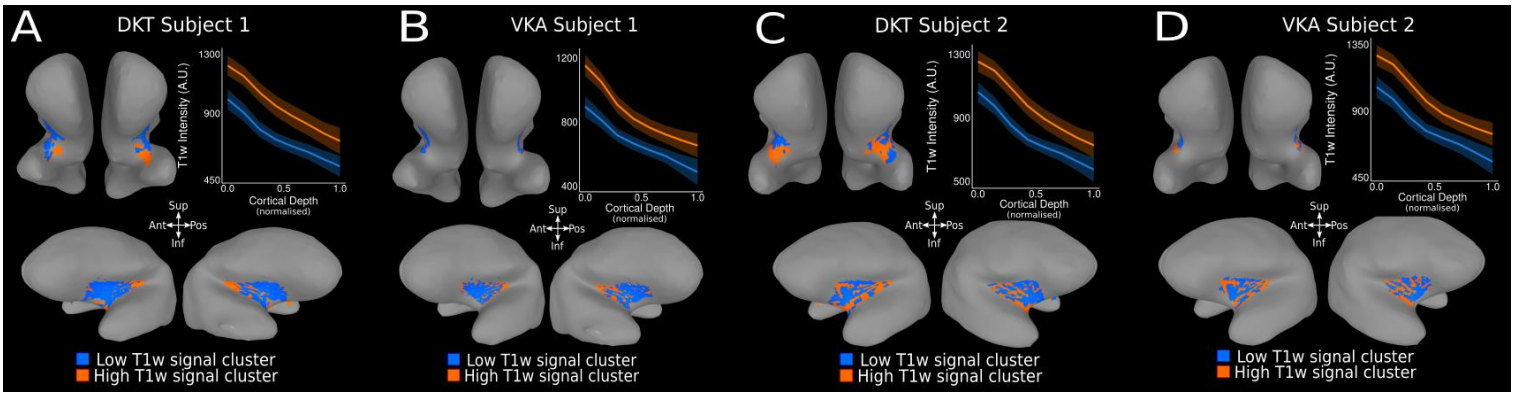

Figure 9, T1-w Intensity Profiles and Clusters in DTK insula ROI for AHEAD Dataset Individuals. ***A.*** *Average high (orange) and low (blue) T1-w intensity profiles for the insula DKT ROI at the individual subject level. T1-w intensity is plotted along cortical depth and clusters are visualised on the MNI SUMA surface of the individual's cortex (high T1-w intensity cluster – orange – and low T1-w intensity cluster – blue –).* ***B.*** *Average high and low T1-w intensity profiles for the insula VKA ROI in the same subject.* ***C-D.*** *Replication of A and B in a second subject example.*

Group-Level T1-w Intensity Profiles and Clusters Withing the DKT Insula ROI of the AHEAD Dataset

Utilising a larger sample from the AHEAD dataset resulted in a broader age range and subsequent increase in anatomical variability. To manage this variability in our group-level analysis, we divided the cohort into two age groups splitting the data in approximately two halves: ages 18-40 (n = 52 participants) and ages 41-80 (n = 49 participants). T1-w signal monotonically decreases along cortical depth in both the high- and low-T1-w signal cluster for participants aged 18-40 (estimate = -433.40, t=-710.20, p<0.001) and participants aged 41-80 (estimate = -446.13, t=-644.31, p<0.001). We observed distinct high- and low-T1-w intensity profiles across DTK insula ROI in both age groups (Figure 10A, B). Statistical analysis confirms a significant difference in intercept (I) and slope (S) in participants aged 18-40 (I: estimate = 249.87, t=398.68, p<0.001; S: estimate =-91.12, t=-88.19, p<0.001) and 41-80 (I: estimate = 227.73, t=363.49, p<0.001; S: estimate =-66.80, t=-64.62, p<0.001). The majority of individual subject's low- (Figure 4C) and high- (Figure 4D) T1-w signal clusters are localised within the same cortical location of the DKT insula ROI. Synonymous with the Glasgow dataset, high T1-w intensity clusters are localised towards the anterior-inferior and posterior-superior DKT insula ROI (Figure 4B,D white arrows) and the low T1-w intensity cluster is localised in the middle region of the DKT insula ROI. Across the population, the high T1-w clusters location occupy 34% of the DKT surface insula ROI (here we defined a high T1-w cluster location across the population as those nodes on the cortical surface where more than 70% of individuals show a high T1-w intensity cluster).

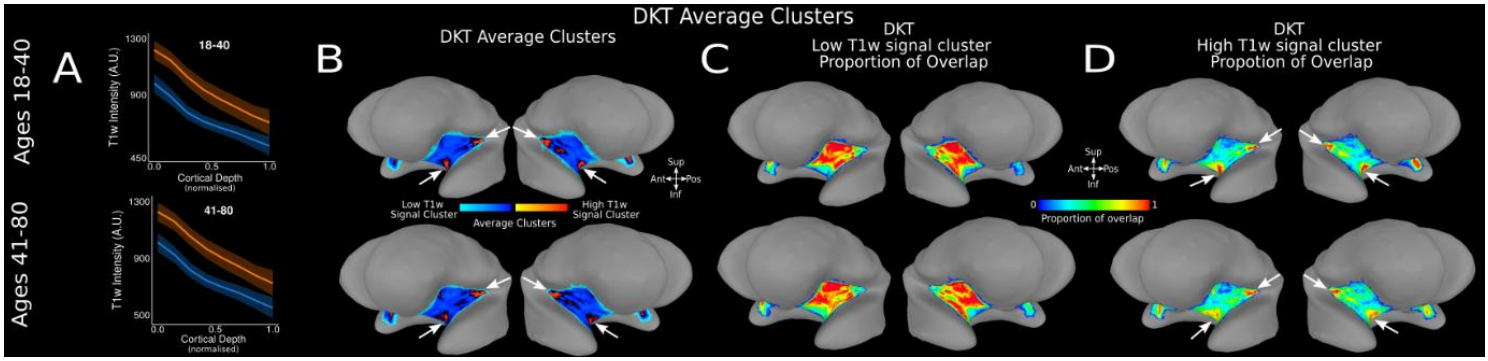

Figure 10, T1-w Intensity Profiles and Clusters in DTK Insula ROI for Two Age Groups in AHEAD Dataset.

A. *Average high (orange) and low (blue) T1-w intensity profiles plotted across cortical depth for the insula DKT ROI in age groups 18-40 (n=52) - panel 1 - and 41-80 (n=49) - panel 2.* ***B.*** *Average clusters across subjects in each age group are visualised on the SUMA MNI surface. White arrows identify two areas of high T1-w signal clusters, located in the posterior-superior and anterior-inferior region of the DKT insula ROI for each age group.* ***C.*** *Proportion of overlap for low-T1-w signal cluster within the insula DKT ROI across each age group, over on the average MNI SUMA surface.* ***D.*** *Proportion of overlap for high T1-w signal cluster for the insula DKT ROI across each age group visualised on the MNI SUMA surface. White arrows identify two areas of high overlap for high-T1-w signal cluster, located in the posterior-superior and anterior-inferior region of the DKT insula ROI.*

Atlas Selection Governs Detection of Anterior T1-w Cluster In AHEAD Dataset

We replicate our findings employing the VKA atlas across the two AHEAD age groups. Distinct high- and low-T1-w intensity profiles are evident across the VKA atlas insula ROI at a group level for both age groups (Figure 11A). As with the DKT atlas, T1-w signal monotonically decreases along cortical depth in both the high- and low-T1-w signal cluster observed on the VKA insula ROI in participants aged 18-40 (estimate = -425.04. t=-1272.60, p<0.001) and participants aged 41-80 (estimate = -441.42, -1120.80, p<0.001. Similarly, statistical analysis confirm a significant difference in intercept (I) and slope (S) in participants aged 18-40 (I: estimate = 247.23, t=761.7, p<0.001; S: estimate =-114.61, t=-214.4, p<0.001) and 41-80 (I: estimate = 229.17, t=680.0, p<0.001; S: estimate =-76.46, t=-137.4, p<0.001). Moreover, a high-T1-w intensity cluster is localised to the posterior-superior section of the VKA insula ROI (Figure 11 B,D white arrow), while the low-T1-w intensity cluster is localised in the middle-anterior region of the VKA insula ROI. However, as with the Glasgow dataset, we could not observe a high-T1-w intensity cluster in the anterior VKA insula ROI for either AHEAD age group, due to the differences in extent towards the anterior section of the brain between the DKT and VKA insula ROI. As described previously, here we define a high T1-w cluster location across the population as those nodes on the VKA cortical surface where more than 70% of individuals show a high T1-w intensity cluster. As with the Glasgow dataset, the high T1-w clusters location only occupy 20% of the VKA surface insula ROI (across the population) likely due to the previously discussed atlas differences.

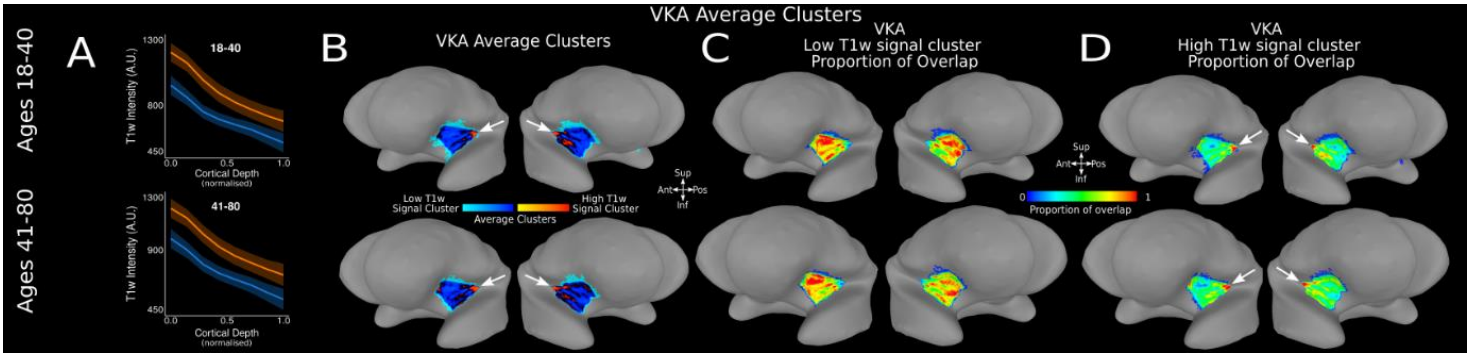

Figure 11: T1-w Intensity Profiles and Clusters in VKA Insula ROI for Two Age Groups in AHEAD Dataset.

A. *Average high (orange) and low (blue) T1-w intensity profiles plotted across cortical depth for the insula VKA ROI in age groups 18-40 (n=52) - panel 1 - and 41-80 (n=49) - panel 2.* ***B.*** *Average clusters across subjects in each age group are visualised on the SUMA MNI surface. White arrow identifies one area of high T1-w signal clusters, located in the posterior-superior of the VKA insula ROI for each age group.* ***C.*** *Proportion of overlap for low-T1-w signal cluster within the insula VKA ROI across each age group, visualised on the average MNI SUMA surface.* ***D.*** *Proportion of overlap for high T1-w signal cluster for the insula VKA ROI across each age group visualised on the MNI SUMA surface. White arrow identifies one area of high overlap for high-T1-w signal cluster, located in the posterior-superior of the VKA insula ROI. High-T1-w intensity cluster in the anterior VKA insula ROI was not observed due to the differences in extent towards the anterior section of the brain between the DKT and VKA insula ROI.*

Summary of Results

Our work offers novel insights into the parcellation of the insula. These findings offer a robust representation of in vivo insula T1-w signal used as a proxy of myelination, both at individual and group levels. When employing the DKT atlas, our results reveal two clusters of high- T1-w profiles in the anterior-inferior and posterior-superior insula locations. Notably, we only observe the high T1-w profiles in the posterior-superior, not the anterior-inferior, insular locations when employing the VKA atlas due to differences in atlas definition. We also confirm the presence of the DKA high T1-w anterior-inferior insular cluster, despite its locality near the potentially confounding MCA. We evidence the two distinct groups of high T1-w profiles are indeed clusters not gradients. These findings are consistent across two cohorts, across different age-groups, acquired from two different sites and scanner vendors.

Discussion

We describe the in-vivo T1-w, cortical depth-dependent profiles of the insula cortex, drawing upon two independent datasets. We use two atlases to localise the insular cortex: the Desikan-Killiany Atlas (DKT) (Desikan et al., 2006) provided by Freesurfer, and the VonEconomo-Koskinas Atlas (VKA) (Scholtens et al., 2018), as employed in Royer et al (2020). The insula ROI from DKT atlas, extended more towards the anterior portion of the brain compared to the VKA atlas. We identify distinct clusters of high- and low-T1-w signal within the insula. These clusters are characterized by distinct offsets in T1-w signal at the level of the individual T1-w profile along cortical depth, and showcase the possibility of performing within-area parcellation using high field imaging, in vivo.

Cortical parcellation has been the target for neuroanatomists since the beginning of the twentieth century, to provide the first steps towards linking local cortical structure to the unknown underlying function (Economo & Koskinas, 1925; Geyer & Turner, 2013; Judas & Cepanec, 2010; Vogt, 1903). Initially, studies were performed ex vivo, on the basis of cortical differences in myeloarchitectonics (the study of myelinated fibres distribution within grey matter, along cortical depth (Judas & Cepanec, 2010; Vogt, 1903)) and cytoarchitectonics (the study of neuronal bodies distribution within grey matter, along cortical depth (Brodmann, 1909)). Today, we can take advantage of modern high field imaging and gain access to cortical structure with an unprecedented level of detail. Here we applied techniques that allows us to gain insights on in vivo parcellation, not only focusing on between-cortical area distinction, but showcasing an example of within-insula parcellation. Furthermore, we show how the within-insula parcellation is robust at the individual and group levels.

DKT and VKA atlases

The differences in insula ROI between the two atlases can be ascribed to the different criteria adopted when defining the boundaries between cortical locations. The DKT atlas is based on a sulcal approach: ROIs were defined by manually tracing from the depth of one sulcus to another, resulting in 34 ROIs overall, per hemisphere, then converted into a standard atlas to automatically label cortical regions. The VKA atlas is based on a digitisation of the original Von Economo and Koskinas work (Economo & Koskinas, 1925), parcellating human neocortex using cytoarchitectonic information, resulting in over 43 cortical regions per hemisphere. Both approaches (DKT and VKA) are valid. For this reason, we decided to perform the analyses and report the results from the insula ROI using both atlases. In the following we discuss the results from both approaches, where relevant. Starting from the DKT atlas, we identify two distinct clusters of high- and low-T1-w signal within the insula. Further analysis reveals how these clusters are localised in three distinct cortical locations within the insula ROI, distributed across its posterior, anterior, and middle sections, with the former two regions notably associated with high levels of T1-w signal along cortical depth. We identify similar clusters starting from the VKA atlas. However, these are distributed in two cortical locations, associated with high- and low-T1-w signal clusters in the posterior and middle-anterior portion of the insula. A second high-myelination cluster cannot be identified in the anterior portion of the VKA insular ROI, due to the lesser extend of the VKA insula ROI towards the anterior portion of the brain compared to the DKT insula ROI.

Comparison with Previous Research

In their seminal study, Royer et al. (2020) used 3T HCP data (Glasser et al., 2013; Van Essen et al., 2013) and identified two primary myelin content gradients within the human insula at a group level: an anterior-to-posterior gradient (G1) and a dorsal-to-ventral gradient (G2). This structural variation supported the functional parcellation of the insula, linking differential myelin distribution to its diverse cognitive and emotional processing functions. In our current study, we used 7T MP2RAGE data employing the VKA atlas (as used in Royer et al., 2020) and observe similar increases in T1-w signal in the posterior-superior region of the insula. Moreover, employing the DKT atlas, we also detect an increase in T1-w signal in the anterior-ventral region. As illustrated by Figure 7, our findings evidence separate clusters of increased T1-w signal. On the other hand, Royer et al. instead documented the presence of T1-w signal gradient between comparable regions of the human insula. The difference between a continuous gradient and separate clusters can be probably ascribed to the single subject analysis approach adopted in the current manuscript, as well as the isotropic, submillimetre spatial resolution of 7T MP2RAGE data.

7T MRI showcases several theoretical benefits over lower field strengths: increased spatial resolution, contrast- and signal-to-noise ratios (CNR and SNR, respectively). Overall, these benefits result in higher quality imaging within comparable acquisition times, which are manifest from a research and clinical perspective (Alkemade et al., 2020; Inglese et al., 2018; Isaacs et al., 2020; Kraff et al., 2015; Peerlings et al., 2019; Trattnig et al., 2018). Importantly, our approach allows for reliable parcellation at both the individual participant and group levels within the insula. In parallel, our identification of increased T1-w signal in the anterior insula using the DKT atlas resonates with existing studies that have emphasised the significance of this cortical location. For example, Evrard's (2019) proposed functional model posits the anterior insula as a hub for integrating incoming information from other intra-insula subregions. Furthermore, Nomi et al. (2018) and Uddin et al. (2017) elaborate on the connections between the anterior insula location and the frontal and limbic regions of the brain, emphasising the importance of these connections in supporting and influencing higher-level cognitive and affective processes.

Previous research has delineated key structural characteristics of the posterior insula, including three distinct cytoarchitectural areas (Kurth et al., 2010), high myelination (Royer et al., 2020), and extensive connections to other cortical regions such as the cingulate, parietal, frontal, and sensorimotor areas of the brain (Nomi et al., 2018; Uddin et al., 2017). These structural features underscore the posterior insula's role in aggregating sensory information and facilitating functions such as temperature and pain perception (Nomi et al., 2018; Uddin et al., 2017). Our observed increase in T1-weighted signal in the posterior insula, as identified using both the DKT and VKA atlases, corroborates Royer et al.'s findings on myelination and provides additional structural insights into this insula's location.

We speculate that the increased T1-w signal we observe in both the posterior and anterior insular regions (using the DKT atlas ROI), could signify their pivotal roles as input and output zones within the insula's network. Through well-myelinated afferent and efferent connections, these regions might facilitate the flow of information to and from other regions within the insula and the surrounding cortical areas. This structural specialisation may be instrumental in supporting the diverse functionality attributed to the posterior and

anterior insula regions, with the mid insula, as noted by Nomi et al. (2018) and Uddin et al. (2017), potentially acting as a transitional region. Our findings align with earlier reports of neuromodulatory and sensory input via connections to sensorimotor regions, thus underscoring its role as a hub for sensory integration (Gogolla, 2017; Klugah-Brown et al., 2023).

Methodological Considerations/ Limitations

T1-weighted imaging largely captures variances in lipid levels, a factor closely linked to myelin presence, yet its signal is also shaped by iron levels in the blood stream and iron-enriched lipids (Fukunaga et al., 2010; Koenig, 1991; Stüber et al., 2014). Consequently, the contrast observed in T1-w images may result from a mix of myelin and iron located within the grey matter.

As part of our analysis, we document that the anterior high myelination profile is adjacent to the nearby middle cerebral artery (MCA) (Türe et al., 2000) (Figure 6). Given the spatial resolution of the MR image voxels to 0.7mm, our results are influenced by the partial volume effect whereby the presence of multiple tissues within a voxel leads to mixed signal intensities. This effect can cause inaccuracies in the representation of tissue boundaries and structures (Billot et al., 2020). Therefore, given the proximity, there is a possibility that the signal from the MCA could alter/confound the intensity of the anterior high myelination profile. As shown in our analysis, the average T1-w profile in the posterior insula cluster differs significantly from the average T1-w profile in the anterior insula cluster with the latter being shallower than the former. However, the proximity of the MCA does not disrupt the overall grey matter segmentation in neighbouring locations, nor does it disrupt the shape of the T1-w profile in the anterior insula cluster (DKT atlas, see Figure 7).

Clinical Relevance & Future Research Directions

These results allow us to gain a deeper understanding of the structural features of the human insula and represent a structural counterpart to the functional tripartite insular parcellation (Menon et al., 2020) under normative conditions. Moreover, given their robustness at the individual level, they represent a promising first step towards an individualised – precision medicine - approach that could find venues of application for clinical populations where the insula appears to be critically involved.

For example, in chronic pain patients, the insula's altered activity correlates with the prolonged experience of pain, reflecting changes in the nociceptive pathway and subsequently how pain is perceived and processed (see McBenedict et al., 2024 for review). Moreover, in inflammatory responses, the insula is pivotal in interpreting nociceptive signals, which can lead to heightened pain sensitivity (Labrakakis, 2023). We speculate that the study of individual myelination profiles could provide greater insights into the insula's role in pain perception and modulation, possibly allowing to differentiate between healthy and pathological states, as well as enable more targeted diagnosis and treatment of patients with pain conditions.

For example, as measured by PET, insula hypometabolism predicts remission with cognitive behaviour therapy and poor response to a selective serotonin reuptake inhibitor antidepressant (escitalopram), while insula hypermetabolism predicts remission with escitalopram and poor response to cognitive behaviour therapy (McGrath et al., 2013).

Moreover, by validating our methodology for characterising individualised insula T1-w profiles, we pave the way for future translational research in precision medicine. In this study, utilising high-resolution 7-tesla imaging allowed us to step away from the traditional 'one-size-fits-all' analytical approach, focusing instead on individual-specific data. This approach requires the development of novel software and analytical methods, tailored to manage this high-resolution data. By prioritising the unique characteristics of each subject's brain structure, we ensure that the specific nuances are thoroughly captured, laying a foundation for personalised treatment planning (Waehnert et al., 2016).

Conclusion

In conclusion, we describe in-vivo T1-w clusters in the anterior and posterior locations of the insula cortex on an individual and group level. We also characterise how application of different atlases can influence the encapsulation of such clusters within the insula. Building from historical approaches on cortical parcellation (Judas & Cepanec, 2010; Nieuwenhuys, 2012b; Vogt, 1903) and modern in vivo imaging techniques (Alkemade et al., 2020; Bock et al., 2013; Glasser & Essen, 2011; Lutti et al., 2013; Royer et al., 2020), our work offers novel insights into the within-insula parcellation in vivo, in humans. These findings offer a robust representation of in vivo insula T1-w signal used as a proxy of myelination, both at individual and group levels, and sets the stage for using insula T1-w profiles for clinical applications as chronic pain and inflammation (Labrakakis, 2023; Rolls, 2023).

References

Alkemade, A., Mulder, M. J., Groot, J. M., Isaacs, B. R., van Berendonk, N., Lute, N., Isherwood, S. J., Bazin, P.-L., & Forstmann, B. U. (2020). The Amsterdam Ultra-high field adult lifespan database (AHEAD): A freely available multimodal 7 Tesla submillimeter magnetic resonance imaging database. *NeuroImage*, *221*, 117200. https://doi.org/10.1016/j.neuroimage.2020.117200

Benarroch, E. E. (2019). Insular cortex: Functional complexity and clinical correlations. *Neurology*, *93*(21), 932–938. https://doi.org/10.1212/WNL.0000000000008525

Billot, B., Robinson, E., Dalca, A. V., & Iglesias, J. E. (2020). Partial Volume Segmentation of Brain MRI Scans of Any Resolution and Contrast. In A. L. Martel, P. Abolmaesumi, D. Stoyanov, D. Mateus, M. A. Zuluaga, S. K. Zhou, D. Racoceanu, & L. Joskowicz (Eds.), *Medical Image Computing and Computer Assisted Intervention – MICCAI 2020* (pp. 177–187). Springer International Publishing. https://doi.org/10.1007/978-3-030-59728-3_18

Bock, N. A., Hashim, E., Janik, R., Konyer, N. B., Weiss, M., Stanisz, G. J., Turner, R., & Geyer, S. (2013). Optimizing T1-weighted imaging of cortical myelin content at 3.0 T. *NeuroImage*, *65*, 1–12. https://doi.org/10.1016/j.neuroimage.2012.09.051

Brodmann, K. (1909). *Vergleichende Lokalisationslehre der Grosshirnrinde in ihren Prinzipien dargestellt auf Grund des Zellenbaues*.

Craig, A. D. (2002). How do you feel? Interoception: the sense of the physiological condition of the body. *Nature Reviews Neuroscience*, *3*(8), 655–666. https://doi.org/10.1038/nrn894

Craig, A. D. (Bud). (2004). Human feelings: Why are some more aware than others? *Trends in Cognitive Sciences*, *8*(6), 239–241. https://doi.org/10.1016/j.tics.2004.04.004

Critchley, H. D., & Garfinkel, S. N. (2017). Interoception and emotion. *Current Opinion in Psychology*, *17*, 7–14. https://doi.org/10.1016/j.copsyc.2017.04.020

Critchley, H. D., & Harrison, N. A. (2013). Visceral Influences on Brain and Behavior. *Neuron*, *77*(4), 624–638. https://doi.org/10.1016/j.neuron.2013.02.008

Critchley, H. D., Wiens, S., Rotshtein, P., Öhman, A., & Dolan, R. J. (2004). Neural systems supporting interoceptive awareness. *Nature Neuroscience*, *7*(2), 189–195. https://doi.org/10.1038/nn1176

de Haan, E. H. F., Scholte, H. S., Pinto, Y., Foschi, N., Polonara, G., & Fabri, M. (2021). Singularity and consciousness: A neuropsychological contribution. *Journal of Neuropsychology*, *15*(1), 1–19. https://doi.org/10.1111/jnp.12234

Desikan, R. S., Ségonne, F., Fischl, B., Quinn, B. T., Dickerson, B. C., Blacker, D., Buckner, R. L., Dale, A. M., Maguire, R. P., Hyman, B. T., Albert, M. S., & Killiany, R. J. (2006). An automated labeling system for subdividing the human cerebral cortex on MRI scans into gyral based regions of interest. *NeuroImage*, *31*(3), 968–980. https://doi.org/10.1016/j.neuroimage.2006.01.021

Droutman, V., Read, S. J., & Bechara, A. (2015). Revisiting the role of the insula in addiction. *Trends in Cognitive Sciences*, *19*(7), 414–420. https://doi.org/10.1016/j.tics.2015.05.005

Economo, C. F. von, & Koskinas, G. N. (1925). Die cytoarchitektonik der hirnrinde des erwachsenen menschen: J. *Julius Springer Verlag*.

Evrard, H. C. (2019). The Organization of the Primate Insular Cortex. *Frontiers in Neuroanatomy*, *13*, 43. https://doi.org/10.3389/fnana.2019.00043

Fischl, B., van der Kouwe, A., Destrieux, C., Halgren, E., Ségonne, F., Salat, D. H., Busa, E., Seidman, L. J., Goldstein, J., Kennedy, D., Caviness, V., Makris, N., Rosen, B., & Dale,

A. M. (2004). Automatically Parcellating the Human Cerebral Cortex. *Cerebral Cortex*, *14*(1), 11–22. https://doi.org/10.1093/cercor/bhg087

Fracasso, A., Dumoulin, S. O., & Petridou, N. (2021). Point-spread function of the BOLD response across columns and cortical depth in human extra-striate cortex. *Progress in Neurobiology*, *207*, 102187. https://doi.org/10.1016/j.pneurobio.2021.102187

Fracasso, A., Luijten, P. R., Dumoulin, S. O., & Petridou, N. (2018). Laminar imaging of positive and negative BOLD in human visual cortex at 7 T. *NeuroImage*, *164*, 100–111. https://doi.org/10.1016/j.neuroimage.2017.02.038

Fracasso, A., Van Veluw, S. J., Visser, F., Luijten, P. R., Spliet, W., Zwanenburg, J. J. M., Dumoulin, S. O., & Petridou, N. (2016a). Lines of Baillarger in vivo and ex vivo: Myelin contrast across lamina at 7 T MRI and histology. *NeuroImage*, *133*, 163–175. https://doi.org/10.1016/j.neuroimage.2016.02.072

Fracasso, A., Van Veluw, S. J., Visser, F., Luijten, P. R., Spliet, W., Zwanenburg, J. J. M., Dumoulin, S. O., & Petridou, N. (2016b). Myelin contrast across lamina at 7T, ex-vivo and in-vivo dataset. *Data in Brief*, *8*, 990–1003. https://doi.org/10.1016/j.dib.2016.06.058

Fukunaga, M., Li, T.-Q., van Gelderen, P., de Zwart, J. A., Shmueli, K., Yao, B., Lee, J., Maric, D., Aronova, M. A., Zhang, G., Leapman, R. D., Schenck, J. F., Merkle, H., & Duyn, J. H. (2010). Layer-specific variation of iron content in cerebral cortex as a source of MRI contrast. *Proceedings of the National Academy of Sciences*, *107*(8), 3834–3839. https://doi.org/10.1073/pnas.0911177107

Gallay, D. S., Gallay, M. N., Jeanmonod, D., Rouiller, E. M., & Morel, A. (2012). The Insula of Reil Revisited: Multiarchitectonic Organization in Macaque Monkeys. *Cerebral Cortex*, *22*(1), 175–190. https://doi.org/10.1093/cercor/bhr104

Gebhardt, S., & Nasrallah, H. A. (2023). The role of the insula in cognitive impairment of schizophrenia. *Schizophrenia Research: Cognition*, *32*, 100277. https://doi.org/10.1016/j.scog.2022.100277

Geyer, S., & Turner, R. (Eds.). (2013). *Microstructural Parcellation of the Human Cerebral Cortex: From Brodmann's Post-Mortem Map to in Vivo Mapping with High-Field Magnetic Resonance Imaging*. Springer Berlin Heidelberg. https://doi.org/10.1007/978-3-642-37824-9

Glasser, M. F., & Essen, D. C. V. (2011). Mapping Human Cortical Areas In Vivo Based on Myelin Content as Revealed by T1- and T2-Weighted MRI. *Journal of Neuroscience*, *31*(32), 11597–11616. https://doi.org/10.1523/JNEUROSCI.2180-11.2011

Glasser, M. F., Sotiropoulos, S. N., Wilson, J. A., Coalson, T. S., Fischl, B., Andersson, J. L., Xu, J., Jbabdi, S., Webster, M., Polimeni, J. R., Van Essen, D. C., Jenkinson, M., & WU-Minn HCP Consortium. (2013). The minimal preprocessing pipelines for the Human Connectome Project. *NeuroImage*, *80*, 105–124. https://doi.org/10.1016/j.neuroimage.2013.04.127

Gogolla, N. (2017). The insular cortex. *Current Biology*, *27*(12), R580–R586. https://doi.org/10.1016/j.cub.2017.05.010

Grady, L. J., & Polimeni, J. (2010). *Discrete calculus: Applied analysis on graphs for computational science*. Springer.

Inglese, M., Fleysher, L., Oesingmann, N., & Petracca, M. (2018). Clinical applications of ultra-high field magnetic resonance imaging in multiple sclerosis. *Expert Review of Neurotherapeutics*, *18*(3), 221–230. https://doi.org/10.1080/14737175.2018.1433033

Isaacs, B. R., Mulder, M. J., Groot, J. M., Berendonk, N. van, Lute, N., Bazin, P.-L., Forstmann, B. U., & Alkemade, A. (2020). 3 versus 7 Tesla magnetic resonance imaging for parcellations of subcortical brain structures in clinical settings. *PLOS ONE*, *15*(11), e0236208. https://doi.org/10.1371/journal.pone.0236208

Judas, M., & Cepanec, M. (2010). Oskar Vogt: The first myeloarchitectonic map of the human frontal cortex. *Translational Neuroscience*, *1*, 72–94. https://doi.org/10.2478/v10134-010-0005-z

Klein, A., & Tourville, J. (2012). 101 Labeled Brain Images and a Consistent Human Cortical Labeling Protocol. *Frontiers in Neuroscience*, *6*. https://doi.org/10.3389/fnins.2012.00171

Klugah-Brown, B., Wang, P., Jiang, Y., Becker, B., Hu, P., Uddin, L. Q., & Biswal, B. (2023). Structural–functional connectivity mapping of the insular cortex: A combined data-driven and meta-analytic topic mapping. *Cerebral Cortex*, *33*(5), 1726–1738. https://doi.org/10.1093/cercor/bhac168

Koenig, S. H. (1991). Cholesterol of myelin is the determinant of gray-white contrast in MRI of brain. *Magnetic Resonance in Medicine*, *20*(2), 285–291. https://doi.org/10.1002/mrm.1910200210

Kraff, O., Fischer, A., Nagel, A. M., Mönninghoff, C., & Ladd, M. E. (2015). MRI at 7 Tesla and above: Demonstrated and potential capabilities. *Journal of Magnetic Resonance Imaging: JMRI*, *41*(1), 13–33. https://doi.org/10.1002/jmri.24573

Kurth, F., Eickhoff, S. B., Schleicher, A., Hoemke, L., Zilles, K., & Amunts, K. (2010). Cytoarchitecture and Probabilistic Maps of the Human Posterior Insular Cortex. *Cerebral Cortex*, *20*(6), 1448–1461. https://doi.org/10.1093/cercor/bhp208

Kurth, F., Zilles, K., Fox, P. T., Laird, A. R., & Eickhoff, S. B. (2010). A link between the systems: Functional differentiation and integration within the human insula revealed by meta-analysis. *Brain Structure and Function*, *214*(5–6), 519–534. https://doi.org/10.1007/s00429-010-0255-z

Labrakakis, C. (2023). The Role of the Insular Cortex in Pain. *International Journal of Molecular Sciences*, *24*(6), 5736. https://doi.org/10.3390/ijms24065736

Lombaert, H., Grady, L., Polimeni, J. R., & Cheriet, F. (2011). Fast brain matching with spectral correspondence. *Information Processing in Medical Imaging: Proceedings of the ... Conference*, *22*, 660–673. https://doi.org/10.1007/978-3-642-22092-0_54

Lutti, A., Dick, F., Sereno, M., & Weiskopf, N. (2013). Using high-resolution quantitative mapping of R1 as an index of cortical myelination. *NeuroImage*, *93*. https://doi.org/10.1016/j.neuroimage.2013.06.005

McBenedict, B., Petrus, D., Pires, M. P., Pogodina, A., Arrey Agbor, D. B., Ahmed, Y. A., Castro Ceron, J. I., Balaji, A., Abrahão, A., & Lima Pessôa, B. (2024). The Role of the Insula in Chronic Pain and Associated Structural Changes: An Integrative Review. *Cureus*. https://doi.org/10.7759/cureus.58511

Medford, N., & Critchley, H. D. (2010). Conjoint activity of anterior insular and anterior cingulate cortex: Awareness and response. *Brain Structure and Function*, *214*(5), 535–549. https://doi.org/10.1007/s00429-010-0265-x

Medrano-Martorell, S., Pumar-Pérez, M., González-Ortiz, S., & Capellades-Font, J. (2021). A review of the anatomy of the middle cerebral artery for the era of thrombectomy: A radiologic tool based on CT angiography and perfusion CT. *Radiología (English Edition)*, *63*(6), 505–511. https://doi.org/10.1016/j.rxeng.2021.10.004

Menon, V., Gallardo, G., Pinsk, M. A., Nguyen, V.-D., Li, J.-R., Cai, W., & Wassermann, D. (2020). Microstructural organization of human insula is linked to its macrofunctional circuitry and predicts cognitive control. *eLife*, *9*, e53470. https://doi.org/10.7554/eLife.53470

Molnar-Szakacs, I., & Uddin, L. Q. (2022). Anterior insula as a gatekeeper of executive control. *Neuroscience & Biobehavioral Reviews*, *139*, 104736. https://doi.org/10.1016/j.neubiorev.2022.104736

Nieuwenhuys, R. (2012a). The insular cortex. In *Progress in Brain Research* (Vol. 195, pp. 123–163). Elsevier. https://doi.org/10.1016/B978-0-444-53860-4.00007-6

Nieuwenhuys, R. (2012b). The Myeloarchitectonic Studies on the Human Cerebral Cortex of the Vogt-Vogt School, and Their Significance for the Interpretation of Functional Neuroimaging Data. *Brain Structure & Function*, *218*. https://doi.org/10.1007/s00429-012-0460-z

Nomi, J. S., Schettini, E., Broce, I., Dick, A. S., & Uddin, L. Q. (2018). Structural Connections of Functionally Defined Human Insular Subdivisions. *Cerebral Cortex*, *28*(10), 3445–3456. https://doi.org/10.1093/cercor/bhx211

Peerlings, J., Compter, I., Janssen, F., Wiggins, C. J., Postma, A. A., Mottaghy, F. M., Lambin, P., & Hoffmann, A. L. (2019). Characterizing geometrical accuracy in clinically optimised 7T and 3T magnetic resonance images for high-precision radiation treatment of brain tumours. *Physics and Imaging in Radiation Oncology*, *9*, 35–42. https://doi.org/10.1016/j.phro.2018.12.001

Rolls, A. (2023). Immunoception: The insular cortex perspective. *Cellular & Molecular Immunology*. https://doi.org/10.1038/s41423-023-01051-8

Royer, J., Paquola, C., Larivière, S., Vos de Wael, R., Tavakol, S., Lowe, A. J., Benkarim, O., Evans, A. C., Bzdok, D., Smallwood, J., Frauscher, B., & Bernhardt, B. C. (2020). Myeloarchitecture gradients in the human insula: Histological underpinnings and association to intrinsic functional connectivity. *NeuroImage*, *216*, 116859. https://doi.org/10.1016/j.neuroimage.2020.116859

Saad, Z. S., & Reynolds, R. C. (2012). SUMA. *NeuroImage*, *62*(2), 768–773. https://doi.org/10.1016/j.neuroimage.2011.09.016

Scholtens, L. H., de Reus, M. A., de Lange, S. C., Schmidt, R., & van den Heuvel, M. P. (2018). An MRI Von Economo – Koskinas atlas. *NeuroImage*, *170*, 249–256. https://doi.org/10.1016/j.neuroimage.2016.12.069

Stüber, C., Morawski, M., Schäfer, A., Labadie, C., Wähnert, M., Leuze, C., Streicher, M., Barapatre, N., Reimann, K., Geyer, S., Spemann, D., & Turner, R. (2014). Myelin and iron concentration in the human brain: A quantitative study of MRI contrast. *NeuroImage*, *93*, 95–106. https://doi.org/10.1016/j.neuroimage.2014.02.026

Tanriover, N., Rhoton, A. L., Kawashima, M., Ulm, A. J., & Yasuda, A. (2004). Microsurgical anatomy of the insula and the sylvian fissure. *Journal of Neurosurgery*, *100*(5), 891–922. https://doi.org/10.3171/jns.2004.100.5.0891

Tisserand, A., Philippi, N., Botzung, A., & Blanc, F. (2023). Me, Myself and My Insula: An Oasis in the Forefront of Self-Consciousness. *Biology*, *12*(4), 599. https://doi.org/10.3390/biology12040599

Trattnig, S., Springer, E., Bogner, W., Hangel, G., Strasser, B., Dymerska, B., Cardoso, P. L., & Robinson, S. D. (2018). Key clinical benefits of neuroimaging at 7T. *NeuroImage*, *168*, 477–489. https://doi.org/10.1016/j.neuroimage.2016.11.031

Türe, U., Yaşargil, M. G., Al-Mefty, O., & Yaşargil, D. C. H. (2000). Arteries of the insula. *Journal of Neurosurgery*, *92*(4), 676–687. https://doi.org/10.3171/jns.2000.92.4.0676

Uddin, L. Q., Kinnison, J., Pessoa, L., & Anderson, M. L. (2014). Beyond the Tripartite Cognition–Emotion–Interoception Model of the Human Insular Cortex. *Journal of Cognitive Neuroscience*, *26*(1), 16–27. https://doi.org/10.1162/jocn_a_00462

Uddin, L. Q., Nomi, J. S., Hébert-Seropian, B., Ghaziri, J., & Boucher, O. (2017). Structure and Function of the Human Insula. *Journal of Clinical Neurophysiology: Official Publication of the American Electroencephalographic Society*, *34*(4), 300–306. https://doi.org/10.1097/WNP.0000000000000377

Van Essen, D. C., Smith, S. M., Barch, D. M., Behrens, T. E. J., Yacoub, E., & Ugurbil, K. (2013). The WU-Minn Human Connectome Project: An Overview. *NeuroImage*, *80*, 62–79. https://doi.org/10.1016/j.neuroimage.2013.05.041

Vogt, O. (1903). Zur anatomischen Gliederung des Cortex cerebri. *J Psychol Neurol*, *2*(4), 160–180.

Waehnert, M. D., Dinse, J., Schäfer, A., Geyer, S., Bazin, P.-L., Turner, R., & Tardif, C. L. (2016). A subject-specific framework for in vivo myeloarchitectonic analysis using high resolution quantitative MRI. *NeuroImage*, *125*, 94–107. https://doi.org/10.1016/j.neuroimage.2015.10.001

Waehnert, M. D., Dinse, J., Weiss, M., Streicher, M. N., Waehnert, P., Geyer, S., Turner, R., & Bazin, P.-L. (2014). Anatomically motivated modeling of cortical laminae. *NeuroImage*, *93*, 210–220. https://doi.org/10.1016/j.neuroimage.2013.03.078